Surface Science 262 (1992) 387–394
North-Holland

surface science

Structure of Au(100) and Au(111) single crystals surfaces prepared by flame annealing

K.M. Robinson [a], I.K. Robinson [b] and W.E. O'Grady [a]

[a] *Code 6170 Chemistry Division, Naval Research Laboratory, Washington, DC 20375, USA*
[b] *AT&T Bell Laboratories, Murray Hill, NJ 07974, USA*

Received 13 June 1991; accepted for publication 7 October 1991

The surfaces of flame annealed Au(111) and Au(100) single crystals have been investigated by synchrotron X-ray diffraction and reflectivity. Electropolished crystals were flame annealed for various lengths of time and studied for structural changes. Electropolishing of the Au(111) and Au(100) crystals produced smooth surfaces with no evidence for reconstructions. Upon flame annealing the Au(111) was slightly roughened, possibly due to stacking fault growth at the surface, while the Au(100) was smoothed with evidence for the hexagonal reconstruction.

1. Introduction

There have been a number of electrochemical and surface reconstruction studies on single crystal Au surfaces [1–8]. The preparation of these surfaces has primarily involved two distinct methods, vacuum annealing–sputtering [1–5] and flame-annealing [6–8]. It was demonstrated that vacuum prepared surfaces can be successfully transferred from the vacuum system to an electrochemical cell while maintaining the prepared surface [1]. A substantial amount of work has been carried out to establish the structure of vacuum prepared Au crystals including LEED [3], RHEED [9] and X-ray diffraction [10,11]. The use of UHV preparation and characterization prevents the use of crystals prepared in this way by a large number of people. On the other hand a number of groups [6–8] have demonstrated that the flame-annealing technique developed by Clavilier [12] leads to consistent reproducible cyclic voltammograms. However very little has been done to confirm the structure of the flame-annealed surfaces. Kolb et al. [6] use the similarity of the double layer capacity of the vacuum prepared and flame-annealed crystals to verify the existence of a (5×20) type structure on a flame-annealed Au(100) although capacitance measurements performed by Hamelin [13] argues against the Kolb results. In the work reported here, synchrotron X-ray radiation has been used to study the structure of flame-annealed Au single crystal surfaces in air.

2. Experimental

The Au crystals were studied by measuring the X-ray specular reflectivity and the crystal truncation rods. The scattering vector is defined for both reflectivity and crystal truncation rods as $\boldsymbol{Q} = \boldsymbol{q}_z + \boldsymbol{q}_{\parallel}$, where $\boldsymbol{q}_z = \boldsymbol{c}^* l$, and $\boldsymbol{q}_{\parallel} = \boldsymbol{a}^* h + \boldsymbol{b}^* k$. The vectors $\boldsymbol{a}^*$, $\boldsymbol{b}^*$ and $\boldsymbol{c}^*$ are the reciprocal lattice vectors for the bulk crystal. For specular reflectivity measurements, $h = k = 0$, while for truncation rods h, k have integer values. The vertical index, l, is not constrained to be integral due to the termination of the bulk crystal [11,14]. The data reported in this paper will use the crystallographic Miller indices, hkl.

Crystal truncation rods, also referred to as non-specular reflectivity, were discovered by Robinson on single crystal surfaces in vacuum

[14]. In reciprocal space, truncation rods are visualized as lines of scattering perpendicular to the terminated surface passing through bulk Bragg peak positions. In real space, the rods can be described as the constructive interference between bulk lattice planes as these planes terminate at the surface where the diffraction constraint on the vertical component of $\boldsymbol{Q}$ is removed. For an abruptly terminated surface the intensity of the rods goes as $1/\Delta q_z^2$, where Δq_z, is the distance, along the q_z direction, from a Bragg reflection. By allowing the surface termination to deviate from an abrupt surface to a rough surface, which can be described by a roughness parameter, β, the intensity of the rod, in q_z, drops more rapidly than the ideal profile. The roughness parameter is described as a layer-to-layer occupancy of atomic positions. Starting with an abruptly terminated surface, the subsequent layer has β occupied sites, the second layer has β^2, and the third has β^3 and so on. As $\beta \to 1$, the surface appears more rough. Similarly, as $\beta \to 0$, the surface approaches an atomically flat surface.

The truncation rod data are fit to [11,14]:

$$|F(q_z)|^2 = N_1^2 N_2^2 \frac{(1-\beta)^2}{[1+\beta^2-2\beta\cos(q_z c)]} \times \frac{1}{4\sin^2(\frac{1}{2}q_z c)}, \quad (1)$$

where N_i^2 are the crystal dimensions in the plane, β is the roughness parameter related to the rms roughness, $\sigma_{\text{rms}} = c\beta^{1/2}/(1-\beta)$ and c is the real space unit cell dimension in the surface normal direction. The calculation of σ_{rms} is only an estimate based on a highly ordered termination, which is not expected in this work, hence only the value of β will be used. The rod data were first visually fit to eq. (1) then a least-squares fit was performed on $N_1^2 N_2^2$ and β. As the intensity from the bulk positions is a constant, $N_1^2 N_2^2$ ($l =$ Bragg reflection) was constrained to a constant value. Incorporating surface reconstruction form factors into the fit had no significant effect on the results.

Specular reflectivity has been used extensively to study density profiles of liquid/vapor interfaces and liquid crystalline surfaces [15]. Solid systems have only recently begun to employ this technique [4,5,16,17]. More precise details concerning the theory of reflectivity are discussed elsewhere [4,5]. Briefly, the reflectivity from the surface is the interference caused by X-ray scattering among the surface layers. By summing the interference from successive layers of the crystalline surface, a reflectivity profile based on single layer deviations from an ideal termination can be constructed. The crystal truncation rod profile, eq. (1), is equivalent to the summing process except that the density variations are characterized by the roughness parameter β. Prior work on Au(100) and Au(111) faces has shown that the first layer gives the most significant contribution to the reflectivity profile [4,5]. Combining these two observations, the specular rod can be fit with eq. (1), which combines bulk roughness effects in β, and a first layer correction for density, dislocation and fluctuation:

$$R(q_z) = |F(q_z, \beta)\ (\text{CTR})|^2 \times |\langle \rho_1 \exp(-q_z^2\sigma_1^2/2) \times \exp[iq_z(a/2)(1-\epsilon_1)]\rangle|^2. \quad (2)$$

The first part of eq. (2) contains the bulk roughness conditions, while the second part of eq. (2) contains the first layer interference terms. The layer density, ρ_1, is relative to the bulk layer density. The layer fluctuation term, σ_1, acts as a first layer Debye–Waller correction. The layer displacement term, ϵ_1, allows the top layer to deviate from the bulk spacing. If the surface were ideally terminated on the crystalline plane with no reconstruction, $\rho_1 = 1$ and $\epsilon_1 = 0$, and the reflectivity profile would appear as an ideal crystal truncation rod. Use of eq. (2) with data presented reports by Gibbs et al. [4] and Ocko et al. [5] gave identical results. In this work, the layer fluctuation term, σ_1, provides only a slight distortion, usually less than the measured experimental error, to the specular rod profile, therefore this term was held constant in the fitting process. In this work, only the surface density, ρ_1, layer displacement term, ϵ_1, and the truncation rod roughness parameter were allowed to vary in a least-squares fit.

The Au crystals (discs of 4 mm diameter × 2 mm thick) were cut from a Au boule (Materials Research corp.), with a bulk FWHM measured on the (111) Bragg peak $< 0.3°$, and aligned by Laue backscattering to $< 0.2°$. The faces were polished using a succession of alumina particles down to 0.33 μm. The crystals were then annealed at 850°C for 12 h in air. Initial X-ray scattering measurements indicated the need for additional polishing, which was done by electropolishing in a 1 : 1 : 2 mixture of glycol : ethanol : HCl (conc.) at 4.5 V [18].

This electropolishing technique removes layers of atoms from the surface. Dropping the voltage to 2–3V produces a very strong etch on the crystal that removes large quantities of the surface [18]. Once a strong surface diffraction intensity was obtained, the crystal was flame annealed and re-electropolished to produce repeatable starting conditions. The crystals were transferred from the laboratory to the beamline in air and mounted onto a standard 4-circle diffractometer, and aligned on low index bulk diffraction peaks. The first set of scans were on the electropolished surfaces. Once the electropolished surface was measured, the crystals were removed from the diffractometer and flame-annealed in a propane torch. The crystals were kept in the flame while red-hot for 10 s. We used two different ways of cooling the crystals. (1) The crystals were rapidly quenched in a beaker of Millipore water or (2) the crystals were allowed to cool approximately 10–15 s before immersion. The first method resulted in the twinning of one sample and was therefore not used further. The flamed crystals were remounted in the diffractometer and realigned on the same bulk Bragg peaks where an identical set of scans were measured.

The X-ray scattering was measured on beamline X-16B at the National Synchrotron Light Source, with fixed wavelength of 1.689 Å. The experimental setup is shown in fig. 1 for reflectivity and truncation rod measurements. The k-space diagrams show the bulk Bragg positions and the rods of scattering. The boxed regions are the reflectivity and truncation rods that were measured on each surface.

The crystal truncation rods and the specular

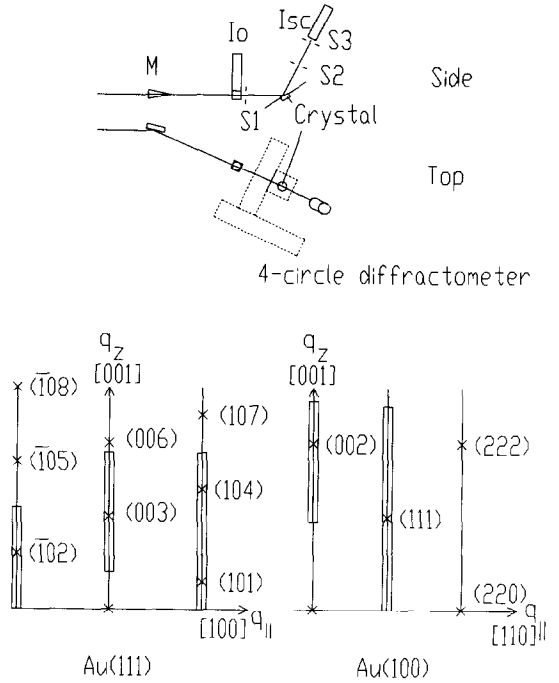

Fig. 1. (a) Top and side views of the experimental setup on beamline 16B. (M) Monochromator crystal, (Io) Beam Monitor, (S1, S2, S3) Slits, (Isc) Scattering Monitor. The 20 arm on the diffractometer is not shown. (b) The reciprocal space representation of crystal truncation rods. The × mark bulk Bragg positions, using indices based on the lattices described in fig. 2 and the lines passing through the × perpendicular to the surface are the truncation rods. The boxed in areas are the regions over which data were collected.

reflectivity were measured by rocking the crystal through a series of (hkl) positions in k-space. The data were background subtracted, integrated and corrected for Lorentz, monitor and geometric factors according to standard procedures [10,11,15]. The integration of the scattered intensity removes detector noise and thermal diffuse scattering from the rod profile, which gives a more accurate determination of the roughness parameter and the reflectivity profile. The polarization correction is 1 with vertical scattering plane. A full set of scans consisted of measurements along the specular reflectivity rod and a low index, usually the (111), truncation rod. The scattering indices from each crystal were defined according to a surface crystalline lattice analogous to LEED measurements. The real and re-

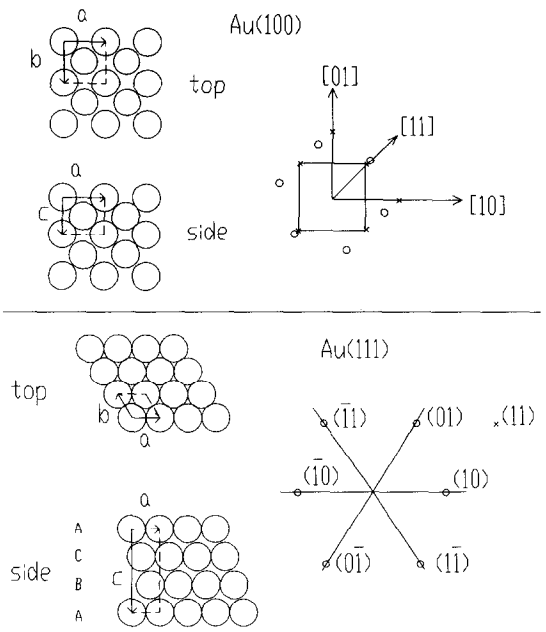

Fig. 2. (a) The surface lattice in real and reciprocal space for Au(100). The × are bulk Bragg positions and the ○ are surface diffraction positions from the 20×5 hexagonal reconstruction (— — —), which is not shown in the real space figure. (b) The surface lattice in real and reciprocal space for Au(111). Similarly, the × mark bulk Bragg positions and the ○ are truncation rods intersecting the surface. The ABC stacking of the (111) interface is shown in the side view.

ciprocal surface lattices are defined in fig. 2 for the two crystal surfaces.

3. Results and discussion

3.1. Au(111)

The reflectivity and crystal truncation rods for the Au(111) electropolished and flame annealed surfaces are shown in figs. 3 and 4, respectively. The reflectivity curves are nearly identical in shape for the electropolished and flamed surfaces. This indicates that there is little difference between the state of the surface before and after flame annealing. The data from the crystal truncation rod also indicates little difference between the two surfaces.

The fits of eqs. (1) and (2) to the data in figs. 3 and 4 are summarized in table 1. The crystal

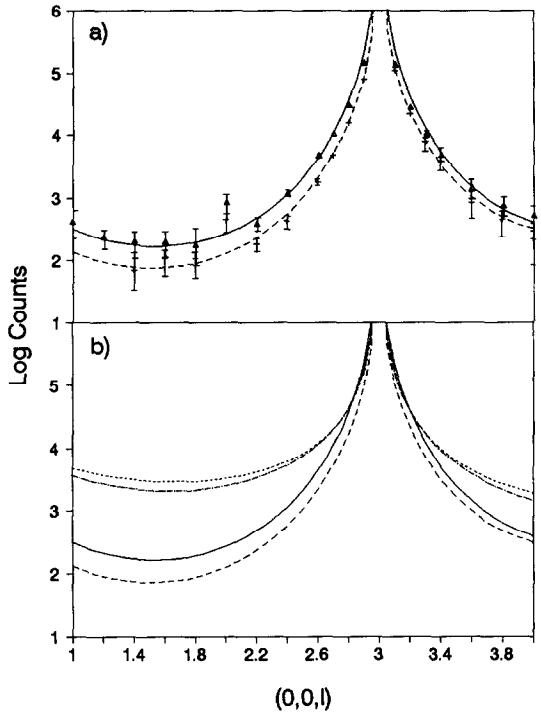

Fig. 3. (a) Reflectivity data for the electropolished (△) and flame annealed (+) Au(111) surfaces. The lines are the best fits for the electropolished (———) and flame annealed surfaces (— — —). The deviation at $l = 2.2$ is due to beamline harmonics. (b) Reflectivity profiles for the electropolished (———), flame annealed (— — —), ideally terminated (· · · · · ·) and $23 \times \sqrt{3}$ reconstructed (· – · – ·) surfaces for Au(111).

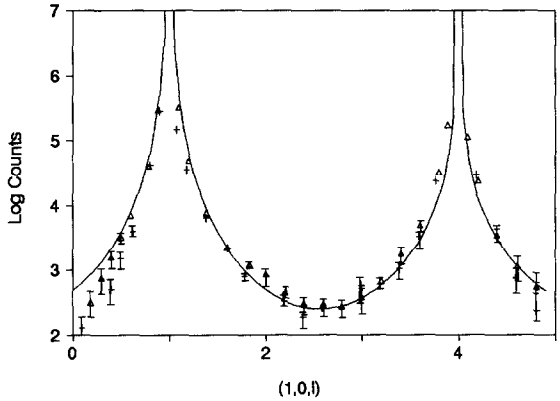

Fig. 4. (101) truncation rod data for the electropolished (△) and flame annealed (+) Au(111) surfaces. The solid line is the best fit for both surfaces. The deviation at low l is due to the low angle of incidence to the surface.

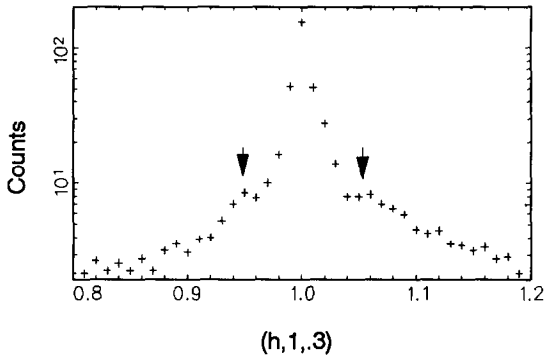

Fig. 5. Wide h scan of the (1, 1, 0.3) truncation rod. The arrows indicate scattering from the $(23 \times \sqrt{3})$ reconstruction.

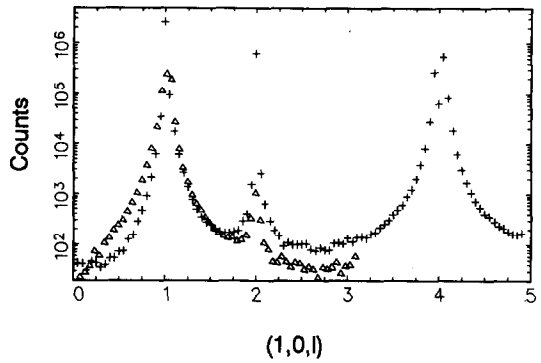

Fig. 6. (101) truncation rod showing the growth of (111) stacking ts as a result of lateral pressure during the flaming process. A slight stacking fault before flaming (△) existed, however after flaming (+) the fault has grown to a size comparable with the bulk diffraction peak.

truncation rods for both the electropolished and flame annealed Au(111) surfaces indicate a surface with a $\beta = 0.3 \pm 0.05$. Both the electropolished and flame annealed surfaces gave a bulk Debye–Waller factor of $\langle u^2 \rangle^{1/2} = 0.09$ Å, which is very similar to the reported bulk value of 0.08 Å [17]. The reflectivity curves indicate that both the electropolished and flame annealed surfaces have an $\epsilon_1 = 1.0 \pm 0.05$ and a density $\rho_1 = 1.0 \pm 0.1$. The error allows no observation of the excess 4.4% atomic surface packing observed at high temperatures [4]. The roughness parameters that were used to fit the reflectivity curves are considerably higher than the truncation rods. The increase in the surface roughness for the reflectivity is possibly due to termination of stacking faults and/or surface buckling, which is a product of the Au(111) reconstruction [1,16]. These effects would not be observed by the truncation rods, which are sensitive to the termination of the bulk planes. A wide scan in h about the (1, 1, 0.3) position, fig. 5, suggests the presence of a $23 \times \sqrt{3}$ surface structure, however the signal-to-noise ratio is insufficient, due to background noise, to further analyze this structure.

As a note of caution, we would like to point out the observation of the growth of stacking faults in one of our Au(111) crystals. During the flame annealing process, the crystals were held by delicate tweezers in the propane torch. In most cases this caused no surface distortions as the surface diffraction of the crystals presented here demonstrates. In one particular Au(111) crystal, a stiffer pair of negative tweezers were used to hold the crystal and this resulted in the growth of stacking faults in the bulk of the crystal as shown in fig. 6. The presence of stacking faults did not change the surface roughness to any major degree, however they did distort the crystal truncation rods sufficiently to prevent a good fitting of the curves. Crystals in which stacking faults were observed were not used to obtain the data presented here.

3.2. Au(100)

The reflectivity and crystal truncation rod for the electropolished and flame annealed Au(100) surfaces are shown in figs. 7 and 8, respectively. It

Table 1
Fitting parameters for the Au(111) crystal truncation rod and reflectivity profiles

	β_{CTR}	$\langle u^2 \rangle^{1/2}$ (Å)	ρ_1	ϵ_1	σ^1	β_{Ref}	$N_1^2 N_2^2$
Polished	0.30 ± 0.02	0.09	1.0 ± 0.1	1.0 ± 0.05	0.1	0.75 ± 0.02	60
Flamed	0.30 ± 0.02	0.09	1.0 ± 0.1	1.0 ± 0.05	0.2	0.80 ± 0.02	120

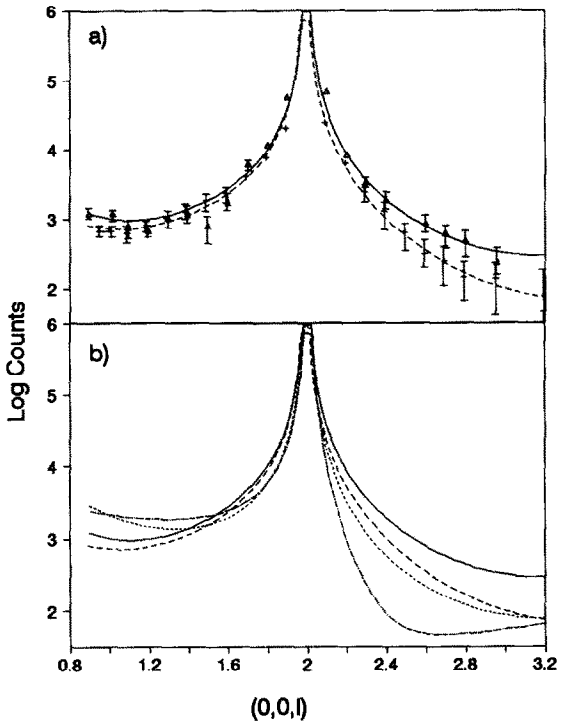

Fig. 7. (a) Reflectivity data for the electropolished (△) and flame annealed (+) Au(100) surfaces. The lines are the best fits for the electropolished (———) and flame annealed surfaces (— — —). (b) Reflectivity profiles for the electropolished (———), flame annealed (— — —), ideally terminated (· · · · · ·) and 5×20 reconstructed (· – · – ·) surfaces for Au(111).

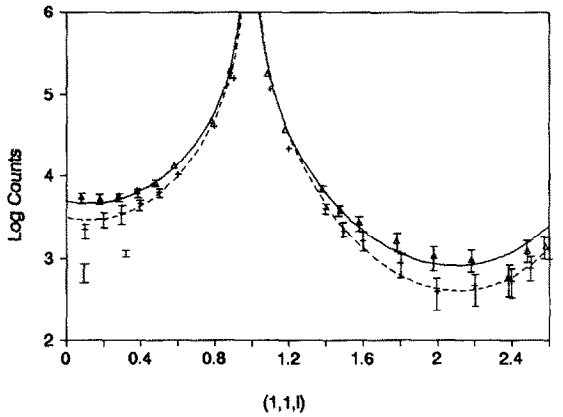

Fig. 8. (111) truncation rod data for the electropolished (△) and flame annealed (+) Au(100) surfaces. The lines are the best fits for the electropolished (———) and flame annealed surfaces (— — —).

is apparent from the data that the flame annealing has altered the Au(100) surface. The data were fit to eqs. (1) and (2) with the parameters in table 2. The reflectivity curve for the electropolished surface was best fit with a $\rho_1 = 1.1 \pm 0.1$ and $\epsilon_1 = 1.0 \pm 0.1$ and a $\beta = 0.3 \pm 0.05$. A bulk Debye–Waller factor of 0.08 Å was fit to the baseline, which is within error of the bulk value. The crystal truncation rod for the electropolished surface was also fit with a $\beta = 0.25 \pm 0.05$. The fits of the reflectivity and the truncation rod describe a relatively flat surface with the possibility of the reconstruction. The data were sufficiently noisy at low l that the fit of the surface density could indicate either the hexagonal top layer or ideally terminated. It is possible that the data reflect an average of the two possibilities since the reconstruction has been observed to have only partial coverage at low (< 523 K) temperatures [2]. Surface diffraction scans at the (1.2, 1.2, 0.3) position, which would indicate large domains of the hexagonal top layer, were featureless.

The reflectivity curve for the flame annealed Au(100) surface was fit with $\rho_1 = 1.18 \pm 0.02$, $\epsilon_1 = 1.16 \pm 0.04$ and a surface roughness of $\beta = 0.10 \pm 0.02$. The crystal truncation rod is fit with a roughness parameter of $\beta = 0.45 \pm 0.08$. The fitting parameters indicate that the surface reconstruction is equivalent to that reported in the vacuum studies [4,5] and describes a hexagonal top layer with a increased surface displacement from the bulk. The surface appears, by reflectiv-

Table 2
Fitting parameters for the Au(100) crystal truncation rod and reflectivity profiles

	β_{CTR}	$\langle u^2 \rangle^{1/2}$ (Å)	ρ_1	ϵ_1	σ^1	β_{Ref}	$N_1^2 N_2^2$
Polished	0.25 ± 0.05	0.08	1.1 ± 0.1	1.0 ± 0.05	0.2	0.30 ± 0.05	380
Flamed	0.45 ± 0.08	0.08	1.2 ± 0.02	1.16 ± 0.02	0.2	0.10 ± 0.02	200

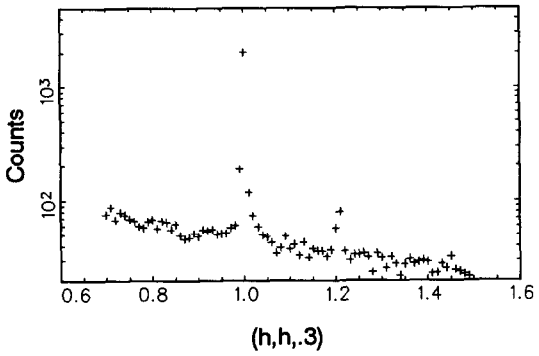

Fig. 9. Wide h, k scan of the (1, 1, 0.3) truncation rod. The large peak at (1, 1, 0.3) is the truncation rod. The second peak at (1.2, 1.2, 0.3) is scattering from the hexagonal overlayer.

ity, to be less rough than the polished surface except for the increased roughness of the truncation rods. This discrepancy can be accounted for by the loss of atoms from the terminated bulk planes to fill small steps in the surface. This would cause the reflectivity to appear smoother at the expense of increased roughness of the truncation rods which are sensitive to the bulk planes. The structure of the filled in steps would probably be hexagonal; a slight increase in the density of the second layer does improve the visual appearance of the fit but does not significantly alter the chi-squared fitting parameter.

The samples which were flamed for different time spans all gave nearly identical reflectivity and truncation rod profiles and the fitting parameters reported are based on the averages of these profiles. Separate scans of the (1.2, 1.2, 0.3) position were also made of these time dependent scans. The scans of the 5 and 10 s flame annealing samples were featureless, however the 30 s scan clearly shows the surface diffraction from the hexagonal top layer, fig. 9. In vacuum prepared surfaces the surface diffraction peak is usually comparable in intensity with the (1, 1, 0.3) bulk truncation rod [4,5,17] which indicates a small domain size compared with the bulk. A rocking scan through the (1.2, 1.2, 0.3) position is much broader, FWHM $\approx 4°$, than the (1, 1, 0.3) truncation rod peak, FWHM $\approx 0.5°$. Although the reflectivity curves support the presence of the reconstruction, only the 30 s flame annealed surface contains direct evidence. This indicates some time dependence to the annealing of the reconstruction by flame annealing. Longer periods of flame annealing may be necessary to produce large domains of the 5×20 surface.

4. Conclusions

It can be concluded from the arguments presented here that flame annealing produces surfaces similar to those prepared in vacuum. Flame annealing the Au(111) surface produces a rough surface possibly composed of stacking faults or the buckled reconstruction observed at higher temperatures [4]. There is no evidence that flame annealing Au(111) enhances the reconstruction. Flame annealing the Au(100) surface produces a hexagonal overlayer reminiscent of the vacuum prepared surfaces, however the domain size of the reconstruction is dependent upon the annealing time. The electrochemical quality of the surfaces produced by flame annealing has previously been documented [7,8,19,20]. Further work on the effect of electrochemical cycling on the surface structure is in progress.

Acknowledgements

This work is supported by the Office of Naval Research. K.M.R. acknowledges the support of the National Research Council Fellowship Program. We would also like to acknowledge AT&T for the use of X-16B and NSLS which is supported by the Department of Energy.

References

[1] M.S. Zei, G. Lehmpfuhl and D.M. Kolb, Surf. Sci. 221 (1989) 23.
[2] Y.F. Liew and G.C. Wang, Surf. Sci. 227 (1990) 190.
[3] W. Telieps, M. Mundschau and E. Bauer, Surf. Sci. 225 (1990) 87.
[4] D. Gibbs, B.M. Ocko, D.M. Zehner and S.G.J. Mochrie, Phys. Rev. B 38 (1988) 7303.
[5] B.M. Ocko, J. Wang, A. Davenport and H. Issacs, Phys. Rev. Lett. 65 (1990) 1466.

[6] D.M. Kolb and J. Schneider, Surf. Sci. 162 (1985) 764.
[7] A. Hamelin, M.J. Sottomayor, F. Silva, S.C. Chang and M.J. Weaver, J. Electroanal. Chem. 295 (1990) 291.
[8] A. Hamelin, in: Modern Aspects of Electrochemistry, Vol. 16, Eds. B.E. Conway, R.E. White and J.O'M Bockris (Plenum, New York, 1985) p. 1.
[9] H. Melle and E. Menzel, Z. Naturforsch. 33 a (1978) 282.
[10] E. Vlieg, I.K. Robinson and K. Kern, Surf. Sci. 233 (1990) 248.
[11] R. Feidenhans'l, Surf. Sci. Rep. 10 (1989) 105.
[12] J. Clavilier, A. Hamelin and G. Valette, C.R. Acad. Sci., Ser. C 265 (1967) 221.
[13] A. Hamelin, private communications.
[14] I.K. Robinson, Phys. Rev. B 33 (1986) 3830.
[15] For a review see, J. Als-Nielsen, in: Surface and Dynamics of Surfaces: Topics in Current Physics, Eds. W. Schommers and P. Blanckenhagen (Springer, New York, 1986) p. 181.
[16] K.G. Huang, D. Gibbs, D.M. Zehner, A.R. Sandy and S.G.J. Mochrie, Phys. Rev. Lett. 65 (1990) 3313.
[17] S.G.J. Mochrie, D.M. Zehner, B.M. Ocko and D. Gibbs, Phys. Rev. Lett. 64 (1990) 2925.
[18] J.L. Whitton and J.A. Davies, J. Electrochem. Soc. 111 (1964) 1347.
[19] A. Hamelin and M.J. Weaver, J. Electroanal. Chem. 209 (1986) 109.
[20] A. Hamelin and M.J. Weaver, J. Electroanal. Chem. 223 (1987) 171.